Journal of Catalysis 272 (2010) 28–36

Contents lists available at ScienceDirect

Journal of Catalysis

journal homepage: www.elsevier.com/locate/jcat

Promoter effect of vanadia on Co/Mo/Al_2O_3 catalyst for deep hydrodesulfurization via the hydrogenation reaction pathway

Ting-Mu Chen [a], Chih-Ming Wang [a], Ikai Wang [a], Tseng-Chang Tsai [b,*]

[a] Department of Chemical Engineering, National Tsing-Hua University, Hsinchu 300, Taiwan, ROC
[b] Department of Applied Chemistry, National University of Kaohsiung, Kaohsiung 811, Taiwan, ROC

ARTICLE INFO

Article history:
Received 13 January 2010
Revised 18 March 2010
Accepted 19 March 2010
Available online 10 April 2010

Keywords:
Deep hydrodesulfurization
Clean fuel
4,6-Dimethyldibenzothiophene
Vanadia oxide promoter
Cobalt–molybdenum sulfide

ABSTRACT

Vanadia containing alumina (V*x*-Al_2O_3) was prepared by the co-precipitation method and used as a catalyst support for Co and Mo oxide (Co–Mo/V*x*-Al_2O_3) in the hydrodesulfurization (HDS) reaction. Incorporation of vanadia in the support shifted the reaction mechanism from the direct desulfurization (DDS) pathway to the hydrogenation (HYD) pathway, and hence promoted the activity of Co and Mo oxide for the HDS reaction of the most sterically hindered compound, 4,6-dimethyldibenzothiophene. Detailed catalyst characterization and catalyst testing showed that the promoter effect of vanadia is due to the synergetic effect of the formation of V–Mo sulfide. A binary powder mixture with intimate contact of Co–Mo/γ-Al_2O_3 and Co–Mo/V*x*-Al_2O_3 could facilitate a concerted reaction involving both HYD and DDS pathways. Such a binary powder mixture was shown to yield a high conversion and excellent sulfur removal efficiency for the most refractory sulfur compounds in the production of clean diesel fuels.

1. Introduction

Combustion of diesel fuel has been identified as one of the major emission sources of polyaromatic hydrocarbons (PAH) in urban areas. As environmental consciousness rises, all countries worldwide introduce more stringent legislation to limit the PAH content of diesel fuels. The European Union set the PAH limit in diesel fuels at 11 wt.% in 2000. The Worldwide Fuel Charter organized jointly by automakers and engine manufacturers proposed to limit the PAH content of diesel below 2 wt.%. In the foreseeable future, a sulfur content as low as 10 ppm and a PAH content not greater than 2% may be proposed in most countries worldwide. Deep hydrogenation of PAH can be catalyzed with noble metal catalysts. Since noble metals are sensitive to sulfur poison, complete removal of sulfur compounds contained in diesel fuel is essential. Furthermore, the sulfur compounds are taken into account as the components of PAH. Desulfurization of DBT simultaneously reduces sulfur element of 17.4 g/mol and PAH of 184.3 g/mol. Therefore, HDS reaction can reduce not only sulfur content but also PAH substantially.

Dibenzothiophene (DBT) and its derivatives are the major sulfur species in diesel and gas oil, in which 4,6-dimethyldibenzothiophene (46DMDBT) is the most refractory compound. Deep hydrodesulfurization (HDS) of DBT and 46DMDBT were widely investigated [1–5]. The low HDS reactivity of 46DMDBT is due to the steric hindrance arisen from the two methyl groups at the 4 and 6 positions of the aromatics rings.

HDS can proceed through either the desulfurization (DDS) or the hydrogenation (HYD) pathway. The activity and selectivity of HDS catalysts are strongly affected by their morphology. Daage and Chianelli [6] proposed a rim-edge model for unsupported MoS_2. They found that the HDS reaction of DBT could take place at both rim and edge sites but that the HYD pathway only occurs on rim sites. For the DBT HDS reaction, Egorova and Prins [7] reported a reaction mechanism in which the HYD pathway involved the π adsorption via aromatic rings and the DDS pathway involved σ adsorption via sulfur atoms. Gates and Topsøe [8] demonstrated that desulfurization of sterically hindered DBTs could be facilitated by means of the HYD pathway rather than the DDS pathway. Through the HYD pathway, DMDBT is hydrogenated into naphthenic compounds in which the methyl groups can rotate freely. Therefore, the steric hindrance of DMDBT can be released, and its sulfur atom is accessible for desulfurization, Nishijima et al. [9] showed that over Al_2O_3-supported catalysts, the reaction route varied with single-layered and multi-layered MoS_2 sites.

Pecoraro and Chianelli reported that vanadium sulfide was inactive in the DBT HDS reaction [10]. Later, Lacroix et al. found that unsupported vanadium sulfide was active in biphenyl hydrogenation [11]. According to DeJonghe et al., toluene hydrogenation over Mo/Al_2O_3 could be promoted by vanadia, and the MoS_2 activity increased with increasing vanadia content [12]. Furthermore, Lacroix et al. observed that MoV catalysts possessed higher hydrogenation and cracking activities than MoS_2 [13]. The authors

* Corresponding author. Fax: +886 7 5919348.
E-mail address: tctsai@nuk.edu.tw (T.-C. Tsai).

0021-9517/$ - see front matter © 2010 Elsevier Inc. All rights reserved.
doi:10.1016/j.jcat.2010.03.015

proposed that electron transfer from vanadium species to the surrounding Mo atom could modify the vanadium–sulfur bond and contribute acidity on the MoV site. Thiollier et al. [14] reported that upon pre-sulfiding, CrNiMo/ZrO_2 catalysts can form highly dispersed Cr_2S_3 species and promote HYD and HDS activity. Vanadium and chromium are neighbors in the Periodic Table, vanadium might have a promotion effect similar to the chromium oxide.

In our previous study, we reported that CoO and MoO_3 supported on a ternary V_2O_5–TiO_2–ZrO_2 oxide showed a higher hydrogenation activity than CoO and MoO_3 supported on alumina [15]. It was also shown that the HYD pathway was greatly enhanced by pre-impregnation of 5 wt.% V_2O_5 on the TiO_2–ZrO_2 support [16]. Furthermore, impregnation of vanadia reduced the activity of CoO and MoO_3 catalysts in DBT HDS reaction but enhanced their activity in 46DMDBT HDS reaction. In this study, the binary oxide support V_2O_5–Al_2O_3 (V*x*-Al_2O_3) prepared with co-precipitation method was used to improve the hydrogenation and cracking activity of Co–Mo catalysts due to enhanced HYD/DDS selectivity. In addition, binary catalyst systems with intimate contact of Co–Mo/γ-Al_2O_3 and Co–Mo/V*x*-Al_2O_3 conducting a concerted reaction involving both HYD and DDS pathways were proposed for deep desulfurization of 46DMDBT.

2. Experimental

2.1. Catalyst preparation

V_2O_5–Al_2O_3 supports with vanadia contents of 0, 10, 20, 25 and 30 wt.% were prepared by the co-precipitation method using ammonium metavanadate (MERCK 99%) and aluminum nitrate (SHOWA 98%) [17]. Ammonium metavanadate aqueous solution of 0.03 M was prepared at 60 °C, and its pH value was adjusted to 3.0 with nitric acid under vigorous stirring. Subsequently, the vanadium solution was mixed with an aqueous solution of 0.08 M aluminum nitrate, and the pH was adjusted to 5.5 using ammonium hydroxide. The solution mixture was aged at room temperature for 1 h, and then filtered and washed several times with de-ionized water. The derived paste was first dried at 110 °C for 2 h, heated by rising the temperature to 550 °C at a heating rate of 2 °C/min, and kept for 10 h. The final solid was denoted as V*x*-Al_2O_3. The number *x* refers to the vanadia content in weight percentage in the V*x*-Al_2O_3.

CoO–MoO_3 catalysts were prepared with stepwise incipient wetness impregnation. First, ammonium heptamolybdate (Merck, >99% purity) was impregnated onto the V*x*-Al_2O_3 sample in 10–20 mesh. The impregnated paste was dried at 110 °C for 12 h and calcined according to the heating program: 110–400 °C with a 1 °C/min ramp, 400 °C for 6 h, then 400–500 °C with a 1 °C/min ramp, and finally 500 °C for 2 h. After cooling to room temperature, the resulting sample was impregnated with cobalt(II) nitrate hexahydrate (Merck, >99% purity) and thermally treated according to the same procedure. The final sample was denoted as Co–Mo/γ-Al_2O_3, Co–Mo/V10-Al_2O_3, Co–Mo/V20-Al_2O_3, Co–Mo/V25-Al_2O_3 and Co–Mo/V30-Al_2O_3 with 2 wt.% CoO and 4 wt.% MoO_3 for each sample.

2.2. Catalyst characterization

The structures of the synthesized supports were determined from their X-ray diffraction (XRD) patterns with a Rigaku RU-H3R X-ray powder diffractometer using Cu Kα radiation. Their specific surface areas, pore volumes and pore size distributions were measured by using a Micrometrics ASAP 2000 instrument. The samples were degassed at 200 °C for 2 h. Nitrogen adsorption and desorption isotherms were obtained at −196 °C. Surface areas were determined by the BET method, and pore size distributions were determined by the BJH method.

X-ray photoelectron spectroscopy (XPS) spectra were obtained by using a PHI Quantera SXM photoelectron spectrometer with Al Kα radiation. The pre-sulfiding procedure was described below in Section 2.3. The pre-sulfided catalyst samples were stored in a vacuum holder and transferred to the XPS chamber as soon as possible to minimize the exposure of those samples from air contact. The charging effect was minimized by using a charge neutralizer and was further corrected by adjusting the C 1s peak to the position of 284.5 eV. The surface elemental composition was determined from the peak areas of the Mo 3d, Co 2p, V 2p, S 2p and S 2s peaks after correction with sensitivity factors provided by the Quantera instrument.

2.3. Catalytic activity test

Activity tests were conducted following the same procedure described earlier [16]. Briefly, the DBT or 46DMDBT was fed into a continuous flow through fixed bed stainless steel micro-reactor. The reactor was loaded with a catalyst sample of 2 g. The catalyst sample was pre-sulfided with a toluene solution containing 6 wt.% of CS_2. The reactor was heated to 250 °C at a heating rate of 50 °C/h, kept at 250 °C for 16 h, then further heated to 350 °C, and finally kept at 350 °C for 24 h under a hydrogen pressure of 2.96 MPa. The HDS reaction was conducted between 280 and 340 °C, at a pressure of 3.43 MPa, a WHSV of 3 h^{-1} and a H_2/HC molar ratio of 8. The synthetic feed contained either 1 wt.% DBT or 1 wt.% 46DMDBT (with sulfur content of 0.17 or 0.15 wt.%), 0.4 wt.% CS_2 (with sulfur content of 0.34 wt.%) and 98.6% mixed solvent (consisting of 1,2,3,4-tetramethylbenzene, toluene and 1,3,5-trimethylbenzene at 1:49.3:49.7 wt. ratio).

The reaction products were sampled and analyzed by a China Chromatograph GC-8700F, equipped with a flame ionization detector and a 0.25 mm × 100 m dimethyl polysiloxane capillary column. Representative GC spectra with identified reaction products were shown elsewhere [16].

3. Results and discussion

3.1. Catalyst characterization

The XRD patterns (not shown here) only showed the specific γ-Al_2O_3 peaks, and the other V*x*-Al_2O_3 supports were X-ray amorphous. Our earlier study showed vanadia of 5 wt.% with impregnation method affected only slightly the textural properties of γ-Al_2O_3 [16]. The vanadia effect with co-precipitation method was examined in this study in wide range of vanadia content. The textural properties of the various supports and supported Co–Mo catalysts are listed in Table 1. The surface area, pore volume and the average pore size of the γ-Al_2O_3 support were 236 m^2/g, 0.49 cc/g and 63 Å, respectively. The textural properties changed remarkably with vanadia content. Compared to the γ-Al_2O_3 support, all the V*x*-Al_2O_3 supports had smaller surface area and larger pore volume. V10-Al_2O_3 had smaller pore diameter and V25- and V30-Al_2O_3 had much larger pore diameters than Al_2O_3. As the vanadia content of V*x*-Al_2O_3 supports increased from 10 to 30 wt.%, the surface area decreased from 164 to 68 m^2/g, while the pore volume increased from 0.20 to 0.45 cc/g.

The BET adsorption isotherms and the pore size distributions of the different supports are shown in Fig. 1. The γ-Al_2O_3 support showed a tri-model pore system comprising a sharp peak centered at 36 Å, a minor one between 47 and 109 Å and a broad one between 138 and 822 Å. On the contrary, all V*x*-Al_2O_3 supports possessed mono-dispersed pore systems. The average pore size

Table 1
Surface areas and pore properties of V*x*-Al_2O_3 supports and supported Co–Mo oxide catalysts.

Support ID	γ-Al_2O_3	V10-Al_2O_3	V20-Al_2O_3	V25-Al_2O_3	V30-Al_2O_3
Surface area (m^2/g)	236	164	133	95	68
Pore volume (cc/g)	0.49 (0.18)[a]	0.20	0.29	0.32	0.45
Average pore diameter (Å)	63 (36)[a]	35	62	111	211
Catalyst ID	Co–Mo/γ-Al_2O_3	Co–Mo/V10-Al_2O_3	Co–Mo/V20-Al_2O_3	Co–Mo/V25-Al_2O_3	Co–Mo/V30-Al_2O_3
Surface area (m^2/g)	219	119	86	86	62
Pore volume (cc/g)	0.47 (0.18)[a]	0.15	0.19	0.27	0.26
Average pore diameter (Å)	66 (36)[a]	36	53	95	139

[a] Counting main pore only (referring to Fig. 1).

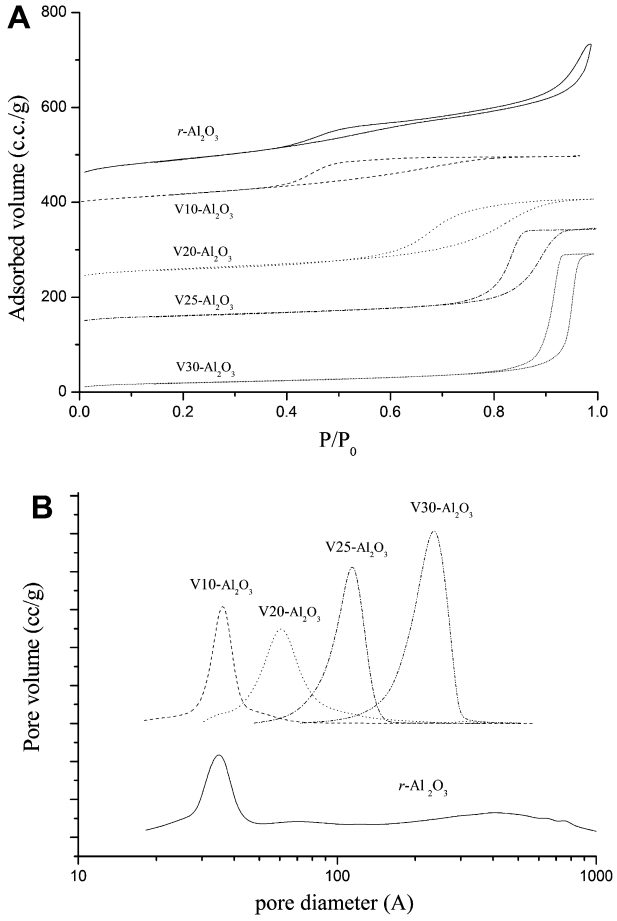

Fig. 1. (A) BET adsorption isotherms. (B) Pore size distributions of V*x*-Al_2O_3 supports.

increased from 35 to 211 Å as the vanadia content increased from 10 to 30 wt.%. Therefore, the pore size of a V*x*-Al_2O_3 support could be adjusted by varying the vanadia content. For example, for considering only the main pore system as shown in Fig. 1, the textural property of the V10-Al_2O_3 support with a main pore diameter of 35 Å and a pore volume of 0.20 cc/g was similar to that of the γ-Al_2O_3 support with a main pore diameter of 36 Å and a pore volume of 0.18 cc/g.

Alumina phase depends on the precipitation conditions. The structure of alumina would be in amorphous phase at pH between 4.0 and 7.5; in pseudo boehmite (γ-AlO(OH)) at pH between 8.0 and 9.5; and in crystalline Bayerite structure at pH between 9.5 and 11 [18]. Blangenois et al. reported that the textural properties and structural phases of V*x*-Al_2O_3 depend on the ion concentration of the metallic solution, precipitation temperature, aging time and pH value in co-precipitation procedure [17]. The change of decreasing surface area, enlarged pore size and pore volume shrinkage with increasing vanadia content in V*x*-Al_2O_3 has been reported [19]. We observed that impregnation of vanadia affected similarly the textural property of TiO_2–ZrO_2 support [16]. Co-precipitation of V*x*-Al_2O_3 conducted in the present study was at pH of 5.5 at which tetrahedral polymeric $[VOx]_n^{n-}$ and amorphous aluminum hydroxide species would form amorphous V–Al–O*x* mixed phase by condensation [17]. The change in textural property of V*x*-Al_2O_3 could be due to partial blockage of vanadia onto the micropore of alumina [19].

The surface area, pore volume and the average pore size of the γ-Al_2O_3 support before and after impregnation with CoO–MoO_3 were about the same. However, the textural properties of the V*x*-Al_2O_3 supports decreased significantly after impregnation with CoO and MoO_3. This might be due to the unstable morphology of the V*x*-Al_2O_3 materials, resulting in pore structure collapse upon repetitive calcination during consecutive loading of CoO and MoO_3.

3.2. XPS spectra

The specific binding energies of the Co 2p, Mo $3d_{5/2}$ and V $2p_{3/2}$ XPS peaks are listed in Table 2. Since the loading of CoO was only 2 wt.%, the intensity of the Co 2p peak was very weak. Nevertheless, the Co 2p binding energy of Co–Mo/γ-Al_2O_3 in the oxidic state and sulfidic state (after pre-sulfiding treatment) could be estimated as 780.4 and 777.6 eV, respectively. The similarity in the Co 2p binding energy among Co–Mo/γ-Al_2O_3 and Co–Mo/V*x*-Al_2O_3 indicated a weak interaction between the CoO and the vanadia species.

The XPS spectra of Mo are shown in Fig. 2. They consisted of three peaks representing the Mo $3d_{5/2}$, Mo $3d_{3/2}$ and S 2s peaks (the latter only appeared after the pre-sulfiding treatment). The Mo $3d_{5/2}$ spectrum was assigned to Mo^{6+} of Mo oxide species (MoO_3) [20]. Furthermore, the upward shift of Mo $3d_{5/2}$ binding energy was attributed to the formation of $Al_2(MoO_4)_3$ [21]. The XPS data showed that the Mo $3d_{5/2}$ peaks shifted to higher binding

Table 2
Binding energies and surface atomic ratios of supported Co–Mo oxide catalysts determined by XPS.

Supports	γ-Al_2O_3	V10-Al_2O_3	V20-Al_2O_3	V25-Al_2O_3	V30-Al_2O_3
Oxidic state					
Co 2p	780.4	780.4	780.4	780.4	780.4
Mo $3d_{5/2}$	232.1	232.1	232.5	232.8	232.7
V $2p_{3/2}$	–	516.7	517.2	517.4	517.3
V/Al	–	0.06	0.16	0.18	0.23
Sulfidic state					
Co 2p	777.6	777.6	777.6	777.6	777.6
Mo $3d_{5/2}$	228.3	228.1	227.8	227.6	228.1
V $2p_{3/2}$	–	515.6	515.4	515.2	515.8
S/Mo	2.92	3.46	3.49	3.62	3.60

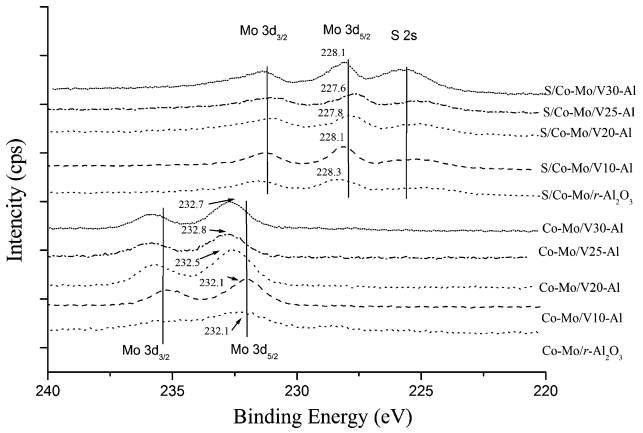

Fig. 2. Mo 3d XPS spectra of Co–Mo/V*x*-Al_2O_3 and pre-sulfided Co–Mo/V*x*-Al_2O_3.

energy in general with increasing vanadia content of the V*x*-Al_2O_3 supports except for the Co–Mo/V30-Al_2O_3 catalyst, indicating a strong interaction between MoO_3 and vanadia. Thiollier et al. [14] reported that Cr–Ni interaction is stronger than Ni–Mo in the CrNiMo/ZrO_2 system. As vanadium and chromium are neighbors in the Periodic Table, vanadium oxide might have similar strong interaction with molybdenum oxide as chromium oxide does. The exceptional Mo $3d_{5/2}$ binding energy of the Co–Mo/V30-Al_2O_3 catalyst might be due to segregation of vanadia in the V30-Al_2O_3 support.

The Mo $3d_{5/2}$ binding energy shifted to lower values after the pre-sulfiding treatment. The molybdenum species could be assigned as Mo^{4+} of MoS_2, or possibly Mo^{3+} in a partially reduced state. The binding energy decreased with the increasing vanadia content in the V*x*-Al_2O_3 supports from 0 to 25 wt.% V (from 228.3 eV for Co–Mo/γ-Al_2O_3 to 227.6 eV for Co–Mo/V25-Al_2O_3), indicating that vanadia affects the interaction between Mo and the V*x*-Al_2O_3 support after sulfidation.

The XPS spectra of V are shown in Fig. 3. They have the same trend as the Mo 3d XPS spectra, the V 2p binding energy of the Co–Mo/V*x*-Al_2O_3 catalyst in the sulfidic form was lower than that in the oxidic form. Furthermore, V 2p binding energy of the oxidic form samples increased in general with increasing vanadia content of the V*x*-Al_2O_3 support except for the Co–Mo/V30-Al_2O_3 catalyst. An opposite trend was found in the sulfided catalysts.

After sulfidation, the binding energy of the V 2p spectra shifted from 516.7–517.4 eV down to 515.6–515.2 eV. The V 2p XPS spectra of the sulfidic catalysts were broader than those of the oxidic

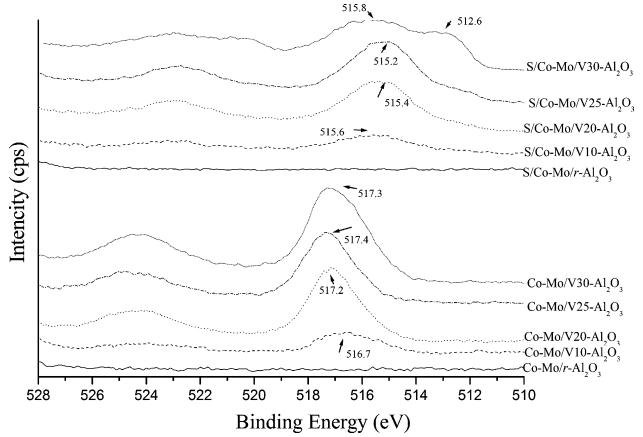

Fig. 3. V 2p XPS spectra of Co–Mo/V*x*-Al_2O_3 and pre-sulfided Co–Mo/V*x*-Al_2O_3.

catalysts, which might be the vanadium sulfides (V_xS_y) formed during the pre-sulfided step. An additional peak appeared at 512.6 eV that was clearly visible for the sulfided Co–Mo/V30-Al_2O_3 catalyst. The Mo $3d_{5/2}$ binding energy of Co–Mo/V30-Al_2O_3 sample was the same as the V-free CoMo/γ-Al_2O_3 sample. The V 2p peaks of the oxidic catalyst could be assigned to V^{4+} and V^{5+} species [22,23], while the additional peak in the V 2p spectrum of the sulfided Co–Mo/V30-Al_2O_3 catalyst could be assigned to V^{2+} of a V–S bond. This discrepancy in XPS with other Co–Mo/V*x*-Al_2O_3 samples, which might due to the excessive V atom in the structure, could explain the different behavior of CoMo/V30-Al_2O_3 sample in DBT HDS reaction, as discussed below.

The Al XPS spectra (not shown here) displayed the same binding energy for all catalysts. In Table 2, the V/Al ratio on the surface was estimated from the XPS spectra of V and Al. In general, the V/Al ratio on the surface was close to that of the bulk composition. The S/Mo ratio on the catalyst surface was estimated from the Mo $3d_{5/2}$, Mo $3d_{3/2}$ and S 2s XPS spectra. The calculated S/Mo ratio of Co–Mo/γ-Al_2O_3 was 2.92, close to the theoretical value (2.96), indicating that CoO and MoO_3 of Co–Mo/γ-Al_2O_3 catalysts were completely sulfided. All the V*x*-Al_2O_3-supported catalysts showed higher S/Mo ratios than Co–Mo/γ-Al_2O_3. The MoS_2 monolayer deposited on catalyst support [6] could have different morphology between γ-Al_2O_3 and V*x*-Al_2O_3 supports. The S/Mo ratios increased with increasing vanadia content to a ceiling of 3.62 for V25-Al_2O_3. The higher sulfur content was attributed to the partial formation of vanadium sulfide, which might change the environment around the Mo species. Having higher surface vanadia content, nevertheless, the S/Mo ratio of V30-Al_2O_3 was the same with V25-Al_2O_3. The exceptional property of V30-Al_2O_3 might be attributed to the segregation of vanadia.

3.3. Catalyst activity

HDS reactions of DBT and 46DMDBT were conducted under the reaction conditions of 300 °C, 3.43 MPa, a WHSV of 3 h^{-1} and a H_2/HC molar ratio of 8. All the catalysts showed mild deactivation in the initial 20 h onstream. After the initial deactivation period, conversion and selectivity remained stable for more than 100 h.

3.3.1. HDS of DBT

The reaction results of the DBT HDS over the V*x*-Al_2O_3 supports and Co–Mo/V*x*-Al_2O_3 catalysts are shown in Tables 3 and 4. The reaction products were classified as desulfurized C_{12} products, undesulfurized products and methylation products. The desulfurized products included biphenyl (BIP), phenylcyclohexane (PCH), dicyclohexyl (DIC), PCH or DIC isomers, such as benzylcyclopentane (benzyl-CP), (cyclopentyl)cyclohexylmethane (CP-CH-methane) and some unidentified products with a molecular weight of 166. The undesulfurized products were the hydrogenation products of DBT without C-S bond scission, including 1,2,3,4-tetrahydro-DBT (THDBT), and hexahydro-DBT (HHDBT) isomers. The CS_2 doped into the feed probably acted as methylation agent [24].

The reaction results of the DBT HDS over the V*x*-Al_2O_3 supports are shown in Table 3. While the γ-Al_2O_3 support had no HDS activity (not shown), the V*x*-Al_2O_3 supports showed moderate catalytic activities, which might come from the V_xS_y species. The DBT conversion and sulfur removal efficiency over the V*x*-Al_2O_3 supports or Co–Mo/V*x*-Al_2O_3 catalysts all increased with increasing vanadia content except for the V30-Al_2O_3 support and the Co–Mo/V30-Al_2O_3 catalyst. Among all V*x*-Al_2O_3 supports, the V25-Al_2O_3 support showed the highest DBT conversion of 36% with a sulfur removal efficiency of 82%.

The DBT HDS reaction can take place via either the HYD or the DDS reaction pathway. A HDS reaction scheme is shown in Fig. 4. The reaction pathway selectivity indexed as HYD/DDS ratio could

Table 3
Product yields of DBT HDS reaction over V*x*-Al_2O_3 supports.[a]

Support	V10-Al_2O_3	V20-Al_2O_3	V25-Al_2O_3	V30-Al_2O_3
DBT conversion (%)	15	33	36	18
S removal efficiency (%)[b]	61	79	82	71
Selectivity (%)				
Desulfurized C_{12} products	60.8	78.7	82.1	70.9
BIP	21.6	23.8	26.7	34.9
PCH	26.3	37.4	39.9	26.7
DIC	5.7	8.0	7.7	3.6
Benzyl-CP	1.1	1.5	1.6	1.5
CP-CH-methane	3.0	4.3	3.9	2.1
Unidentified[c]	3.1	3.7	2.3	2.1
Undesulfurized products	37.9	21.0	17.4	28.0
THDBT (MW 188)	27.0	14.8	12.0	19.4
HHDBT (MW 190)	8.4	4.6	3.9	6.2
Isomeric HHDBT (MW 190)	2.5	1.6	1.5	2.4
Methylation products	1.3	0.2	0.4	1.1
MPCHs	0.0	0.0	0.1	0.1
MBIPs	0.0	0.0	0.0	0.1
MDBTs	1.3	0.2	0.3	0.9
HYD/DDS[d]	3.6	3.2	2.7	1.9
$k_{overall}$[e]	0.5	1.2	1.4	0.6
k_{HYD}[e]	0.4	0.9	1.0	0.4
k_{DDS}[e]	0.1	0.3	0.4	0.2

[a] Reaction conditions: 300 °C, 3.43 MPa, WHSV = 3 h^{-1}, H_2/HC = 8 mol/mol.
[b] S removal efficiency: selectivity of all desulfurized products.
[c] Unidentified desulfurized C_{12} products, MW 166.
[d] HYD/DDS: selectivity of (1-BIP)/selectivity of BIP.
[e] *k* value was estimated according to Eqs. (2)–(4).

be determined from product selectivity as below and used to identify the preferential reaction pathway.

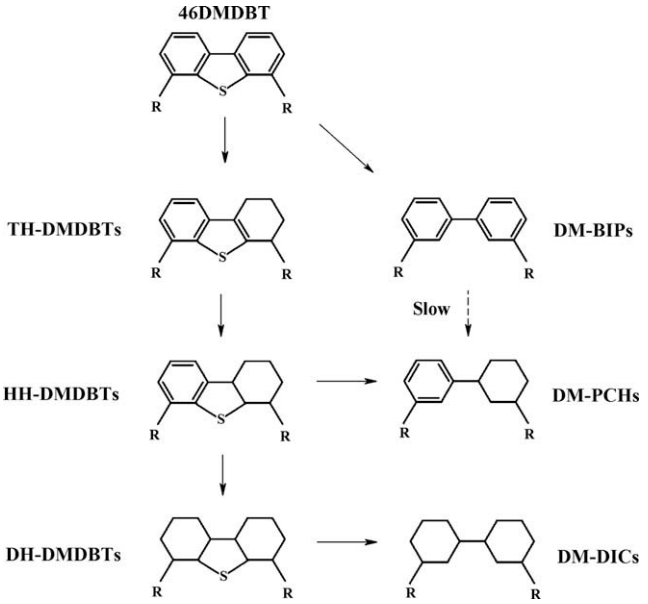

Fig. 4. HDS reaction scheme of 46DMDBT.

$$\text{HYD/DDS ratio} = \text{Selectivity of } (1-\text{BIP})/\text{selectivity of BIP} \quad (1)$$

The HYD/DDS ratios of V10-Al_2O_3, V20-Al_2O_3, V25-Al_2O_3 and V30-Al_2O_3 were 3.6, 3.2, 2.7 and 1.9, respectively (Table 3). Thus, vanadia can promote the HYD pathway by means of vanadium sulfide active sites. At 300 °C, the HDS reaction over the Co–Mo/V*x*-Al_2O_3 catalysts and V*x*-Al_2O_3 supports produced some undesulfurized products, indicating that the HDS activities of the V*x*-Al_2O_3 supports were relatively weak in breaking the C–S bond. Nevertheless, the activity of the Vx-Al_2O_3 support could be enhanced by incorporation of Co–Mo oxides. It is worth noting that the effect of the vanadia content on

Table 4
Product yields of DBT HDS reaction over CoO–MoO_3 supported on γ-Al_2O_3 and V_2O_5–Al_2O_3.[a]

Catalyst	Co–Mo/γ-Al_2O_3	Co–Mo/V10-Al_2O_3	Co–Mo/V20-Al_2O_3	Co–Mo/V25-Al_2O_3	Co–Mo/V30-Al_2O_3
DBT conversion (%)	~100	27	53	60	47
S removal efficiency (%)[b]	~100	88	85	86	79
Selectivity (%)					
Desulfurized C_{12} products	99.7	88.3	84.8	86.2	78.9
BIP	86.6	48.1	26.3	22.9	21.2
PCH	11.7	31.5	39.0	39.1	34.9
DIC	0.2	1.0	4.6	6.9	7.4
Benzyl-CP	0.1	2.5	3.4	3.4	2.7
CP-CH-methane	0.1	1.3	6.0	8.2	7.4
Unidentified[c]	1.0	3.9	5.5	5.7	5.3
Undesulfurized products	0.0	8.8	13.8	12.8	21.2
THDBT (MW 188)	0.0	6.3	9.7	8.9	14.4
HHDBT (MW 190)	0.0	1.9	3.1	2.9	4.7
Isomeric HHDBT (MW 190)	0.0	0.6	1.0	1.0	2.1
Methylation products	0.0	2.8	1.4	1.0	0.0
MPCHs	0.0	0.6	0.6	0.4	0.0
MBIPs	0.0	0.4	0.2	0.2	0.0
MDBTs	0.0	1.8	0.6	0.4	0.0
HYD/DDS[d]	0.2	1.1	2.8	3.4	3.7
$k_{overall}$[e]	17.4	1.0	2.3	2.7	1.9
k_{HYD}[e]	2.3	0.5	1.7	2.1	1.5
k_{DDS}[e]	15.1	0.5	0.6	0.6	0.4

[a] Reaction conditions: 300 °C, 3.43 MPa, WHSV = 3 h^{-1}, H_2/HC = 8 mol/mol.
[b] S removal efficiency: selectivity of all desulfurized products.
[c] Unidentified desulfurized C_{12} products, MW 166.
[d] HYD/DDS: selectivity of (1-BIP)/selectivity of BIP.
[e] *k* value was estimated according to Eqs. (2)–(4).

the HYD/DDS ratio over the V*x*-Al_2O_3 support is opposite to that over the Co–Mo/V*x*-Al_2O_3 catalyst.

As shown in Table 4, the Co–Mo/γ-Al_2O_3 catalyst could almost completely convert DBT and remove sulfur. The desulfurized product was mostly BIP (87%), yielding a HYD/DDS ratio of 0.2. Accordingly, Co–Mo/γ-Al_2O_3 catalyzed the DBT HDS reaction by going mainly through the DDS pathway rather through the HYD pathway.

Interestingly, when vanadia was added to the Al_2O_3 support, the DBT conversion over Co–Mo/V*x*-Al_2O_3 dropped and the HYD/DDS ratio increased remarkably. For example, the 100% DBT conversion over Co–Mo/γ-Al_2O_3 was higher than the 27% conversion over the Co–Mo/V10-Al_2O_3 catalyst. The DBT conversion increased with increasing vanadia content of the V*x*-Al_2O_3 support except for Co–Mo/V30-Al_2O_3. The sulfur removal efficiency of the Co–Mo/V30-Al_2O_3 catalyst was lower than that of any of the other three V-containing catalysts. All the Co–Mo/V*x*-Al_2O_3 catalysts showed much higher THDBT and HHDBT yields than Co–Mo/γ-Al_2O_3 in compensation of the BIP yield. The HYD/DDS ratios over the Co–Mo/V10-Al_2O_3, Co–Mo/V20-Al_2O_3, Co–Mo/V25-Al_2O_3 and Co–Mo/V30-Al_2O_3 catalysts were 1.1, 2.8, 3.4 and 3.7, respectively. The higher HYD/DDS ratios clearly indicated the preference of the HYD pathway over the Co–Mo/V*x*-Al_2O_3 catalysts.

The HDS kinetics can be described as pseudo-first-order reaction [25,26], and the reaction constants of the HYD and DDS pathways, k_{HYD} and k_{DDS}, can be obtained experimentally from the overall rate constants and the selectivity data [27]. According to our previous research [28], we could calculate the apparent overall rate constants by the following equation

$$k_{overall} = \mathrm{WHSV} \times [-ln(1 - X)] \quad (2)$$

where X refers to the conversion of HDS. The HDS and DDS are competing reactions. Thus, the overall speed constant is the summation of k_{HYD} and k_{DDS}, and the rate constant k_{HYD} and k_{DDS} can be determined from the overall rate constants and the HYD/DDS ratio as below,

$$k_{HYD} = k_{overall} * \mathrm{HYD/DDS\ ratio}/(1 + \mathrm{HYD/DDS\ ratio}) \quad (3)$$

$$k_{DDS} = k_{overall} - k\mathrm{HYD} \quad (4)$$

The apparent rate constants of the HYD and DDS pathways are shown in Tables 3–5. The k_{HYD} of DBT HDS via the HYD pathway was larger than k_{DDS} via the DDS pathway for both the V*x*-Al_2O_3 supports and Co–Mo/V*x*-Al_2O_3 catalysts and vice versa for the Co–Mo/γ-Al_2O_3 catalyst.

The effect of vanadia in the V*x*-Al_2O_3 support on the catalytic performance could be attributed to a change of the reaction pathway. Upon incorporation of vanadia into the Co–Mo/V*x*-Al_2O_3 catalysts, the binding energy of Mo in the sulfided state decreased with the increasing vanadia content. The lower binding energy might imply that Mo was easier to sulfide and desulfurize. In addition, the γ-Al_2O_3 support possessed medium and large pores, which could be helpful in the DBT conversion. The lower DBT conversions over the Co–Mo/V*x*-Al_2O_3 catalysts were due to the reduction in DDS activity leading to decreased k_{DDS}. In reference to the Co–Mo/γ-Al_2O_3 catalyst, the k_{DDS} of Co–Mo/V*x*-Al_2O_3 catalysts decreased from 15.1 to about 0.5 by a factor of about 30. Among the Co–Mo/V*x*-Al_2O_3 catalysts, the pre-sulfided Co–Mo/V25-Al_2O_3 had the lowest binding energy of Mo 3d and V 2p and yielded a high HYD/DDS ratio. In conjunction with a large pore system, the Co–Mo/V25-Al_2O_3 showed the maximum k_{HYD} rate constant and conversion for the DBT HDS reaction.

V-containing support promotes the formation of a thin layer of $CoMoS_x$ or of rim sites in supported Co–Mo catalysts that favors the HYD pathway [6,16]. The favorable HYD pathway, with a high HYD/DDS ratio over the V*x*-Al_2O_3 supporting catalysts, as discussed earlier, could be mainly due to the synergetic effect of the formation of binary V–Mo sulfides and the acid nature of the V-containing supports [13]. CoMo/V30-Al_2O_3 sample behaved differently with other Co–Mo/V*x*-Al_2O_3 in DBT HDS reaction. Its XPS spectra show an additional peak at 512.6 eV (Fig. 3), which is attributed to V–S in V_xS_y species. The different catalytic behavior of CoMo/V30-Al_2O_3 could be attributed to the contribution of separate V_xS_y species.

The effect of reaction temperature on the catalytic performance of the Co–Mo/V25-Al_2O_3 catalyst is shown in Table 5. The sulfur removal efficiency was enhanced by raising the reaction temperature. As the reaction temperature increased from 280 to 340 °C, the DBT conversion rose from 28% to 94% and the HYD/DDS ratio decreased from 3.5 to 1.6 with substantial reduction in the yield of undesulfurized products. This result was consistent with the earlier study [27]. Both the k_{DDS} and k_{HYD} increased with the increasing temperature, and the k_{DDS} showed a large increasing rate than k_{HYD}. Assuming first-order kinetics, the activation energy of the DDS and the HYD route were about 31 and 22 kcal/mol. The reduction in HYD pathway selectivity with increasing reaction temperature can be attributed to unfavorable hydrogenation due to thermodynamics or to a higher activation energy for the DDS reaction than for the HYD reaction [29]. Within the whole reaction temperature range, the HYD/DDS ratio over Co–Mo/V25-Al_2O_3 was much higher than the value of 0.2 of the Co–Mo/γ-Al_2O_3 catalyst.

Table 5
Product yields of DBT HDS reaction over Co–Mo/V25-Al_2O_3 at different reaction temperatures.[a]

Temperature (°C)	280	300	320	340
DBT conversion (%)	28	60	86	94
S removal efficiency (%)[b]	69	86	97	99
Selectivity (%)				
Desulfurized C_{12} products	68.6	86.2	96.4	97.9
BIP	22.3	22.9	28.2	38.4
PCH	31.1	39.1	39.4	35.0
DIC	4.6	6.9	6.5	4.9
Benzyl-CP	2.0	3.4	4.6	5.2
CP-CH-methane	4.8	8.2	8.9	7.2
Unidentified[c]	3.8	5.7	8.8	7.2
Undesulfurized products	30.3	12.8	2.7	0.8
THDBT (MW 188)	19.4	8.9	2.1	0.6
HHDBT (MW 190)	8.9	2.9	0.5	0.1
Isomeric HHDBT (MW 190)	2.0	1.0	0.1	0.1
Methylation products	1.0	1.0	1.1	1.4
MPCHs	0.2	0.4	0.6	0.7
MBIPs	0.1	0.2	0.3	0.5
MDBTs	0.7	0.4	0.2	0.2
HYD/DDS[d]	3.5	3.4	2.5	1.6
$k_{overall}$[e]	1.0	2.7	5.8	8.4
k_{HYD}[e]	0.8	2.1	4.2	5.2
k_{DDS}[e]	0.2	0.6	1.6	3.2

[a] Reaction conditions: 3.43 MPa, WHSV = 3 h^{-1}, H_2/HC = 8 mol/mol.
[b] S removal efficiency: selectivity of all desulfurized products.
[c] Unidentified desulfurized C_{12} products, MW 166.
[d] HYD/DDS: selectivity of (1-BIP)/selectivity of BIP.
[e] *k* value was estimated according to Eqs. (2)–(4).

3.3.2. HDS of 46DMDBT

The catalytic performances of Co–Mo/γ-Al_2O_3, Co–Mo/V25-Al_2O_3 and binary catalyst systems, either in complete-mixing mode or in dual-bed mode, for the HDS reaction of the 46DMDBT are compared in Table 6. The products could be classified into three groups of desulfurized C_{14} products, undesulfurized products and cracking products. The cracking products were toluene, naphthenes and multi-branched iso-paraffin [16]. The conversion of the

Table 6
Product yields of 46DMDBT HDS reaction over supported Co–Mo catalysts and binary catalyst systems.[a]

	Single-bed catalyst		Dual-bed catalyst system		Binary catalyst system[b,c]		
Top bed	Co–Mo/γ-Al_2O_3	Co–Mo/V25-Al_2O_3	Co–Mo/γ-Al_2O_3	Co–Mo/V25-Al_2O_3	Co–Mo/γ-Al_2O_3+Co–Mo/V25-Al_2O_3	Co–Mo/γ-Al_2O_3///	Co–Mo/γ-Al_2O_3///
Bottom bed			Co–Mo/V25-Al_2O_3	Co–Mo/γ-Al_2O_3		Co–Mo/V25-Al_2O_3	Co–Mo/V25-Al_2O_3
WHSV (h^{-1})	3	3	3	3	3	3	1.5
Conversion (%)	74	81	76	71	85	87	~100
S removal efficiency (%)[d]	97	81	81	95	93	95	98
Selectivity (%)[e]							
Cracking products	0.0	23.2	6.8	11.5	15.2	2.9	10.1
Desulfurized products	97.4	57.5	74.1	83.7	77.7	92.2	87.9
DM-BIPs (MW 182)	10.9	4.0	7.1	6.0	5.3	4.6	4.7
DM-PCHs (MW 188)	75.5	15.1	41.0	52.1	49.5	63.4	63.4
DM-DICs (MW 194)	10.3	37.1	24.0	23.7	22.0	23.4	18.5
Unidentified	0.7	1.3	2.0	1.9	0.9	0.9	1.3
Undersulfurized products	2.7	19.4	19.1	4.6	7.2	4.9	1.9
DBT	0.0	1.1	0.2	0.0	0.1	0.1	0.0
4M-DBT	0.1	0.1	0.5	0.1	0.2	0.8	0.0
TH-DMDBTs (MW 216)	1.2	10.1	11.0	2.2	4.4	2.2	0.9
HH-DMDBTs (MW 218)	0.6	5.9	6.2	1.9	1.9	1.1	0.7
DH-DMDBTs (MW 224)	0.3	1.2	0.6	0.0	0.2	0.0	0.2
Isomeric DMDBTs	0.5	1.0	0.6	0.4	0.4	0.6	0.1

[a] Reaction conditions: 300 °C, 3.43 MPa, H_2/HC = 8 mol/mol.
[b] Co–Mo/γ-Al_2O_3 + Co–Mo/V25-Al_2O_3 particle mixture.
[c] Co–Mo/γ-Al_2O_3///Co–Mo/V25-Al_2O_3 powder mixture.
[d] S removal efficiency: selectivity of all desulfurized products.
[e] The suffix "s" presents the products included themselves and their isomers.

46DMDBT HDS reaction over Co–Mo/γ-Al_2O_3 was 74% with a sulfur removal efficiency of 97%, lower than the result of the DBT HDS reaction (Table 4). Kabe et al. proved that dimethyl-biphenyl (DMBIP) is the HDS product of 46DMDBT by means of DDS route [3]. Röthlisberger and Prins showed that the conversion of DMBIP to dimethyl-phenylcyclohexane (DMPCH) is slow [29]. Therefore, as shown in Fig. 4, the product selectivity of DM-BIPs could be used as an indicator of the DDS pathway and that of TH-, HH- and DH-DMDBTs as an indicator for the HYD pathway. The much lower DM-BIPs selectivity in using 46DMDBT than the BIP selectivity in using DBT feed (11% vs. 87%) suggested that the 46DMDBT HDS reaction was highly sterically hindered in the DDS pathway. The product selectivities of TH-, HH-, and DH-DMDBTs for the 46DMDBT HDS reaction were significantly higher than the selectivities of their counterparts in the DBT feed (Table 4), indicating that 46DMDBT conversion favors the HYD pathway.

Interestingly, the 46DMDBT conversion of 81% was higher than the DBT conversion of 60% over the Co–Mo/V25-Al_2O_3 catalyst and is associating with a high yield for cracking products. While the selectivity of DM-BIPs in the 46DMDBT HDS reaction was relatively lower than the BIP selectivity in the DBT HDS reaction, the selectivity of the hydrogenated products TH-, HH- and DH-DMDBTs was significantly higher. Accordingly, the 46DMDBT HDS reaction over the Co–Mo/V25-Al_2O_3 catalyst goes mainly through the HYD pathway.

Röthlisberger et al. observed that the hydrogenation route over the Pt–Pd/γ-Al_2O_3 catalysts was faster for 4,6-DM-DBT than for DBT, which can compensate the loss of activity via the desulfurization pathway [30]. The assisted 46DMDBT conversion by the HYD pathway can be attributed to the relaxation of steric hindrance. In the HYD pathway, the 46DMDBT molecular is adsorbed via π adsorption [7,25,27,31,32], hydrogenated into naphthenic sulfur compounds such as TH-, HH- and DH-DMDBTs and then desorbed from the catalyst surface to form reaction products. The steric hindrance of 46DMDBT would be eliminated once it is converted into naphthenic compounds. Then, the naphthenic sulfur compounds could be easily desulfurized in the DDS pathway via σ adsorption. As a result, with high hydrogenation activity, the conversion of 46DMDBT was higher than that of DBT. Nevertheless, with low desulfurization selectivity, the Co–Mo/V25-Al_2O_3 catalyst showed a higher 46DMDBT conversion but a lower sulfur removal efficiency than the Co–Mo/γ-Al_2O_3 catalyst.

As shown in Table 6, at the same WHSV of 3 h^{-1} (based on the total amount of catalyst), the catalytic performance of the dual-bed catalyst system was compared with the single-bed catalyst. Notice that the true WHSV for individual Co–Mo/V25-Al_2O_3 or Co–Mo/γ-Al_2O_3 in the dual-bed catalyst system was doubled. The dual-bed catalyst system, using Co–Mo/γ-Al_2O_3 as a top bed and Co–Mo/V25-Al_2O_3 as a bottom bed (denoted as Co–Mo/γ-Al_2O_3||Co–Mo/V25-Al_2O_3), gave a sulfur removal efficiency of 81% and a conversion of 76%. The sulfur removal efficiency was lower than that over Co–Mo/γ-Al_2O_3 and the conversion was lower than that over the Co–Mo/V25-Al_2O_3 catalyst. The dual-bed catalyst in reversed form (denoted as Co–Mo/V25-Al_2O_3||Co–Mo/γ-Al_2O_3) showed a conversion less than that over a single-bed catalyst of Co–Mo/γ-Al_2O_3 or Co–Mo/V25-Al_2O_3, a sulfur removal efficiency close to that over Co–Mo/γ-Al_2O_3, but higher than that over Co–Mo/V25-Al_2O_3.

The product composition over the dual-bed catalyst systems reflected a concerted DDS and HYD reaction pathway. Over Co–Mo/γ-Al_2O_3||Co–Mo/V25-Al_2O_3, the product composition of desulfurized products was closer to that over Co–Mo/γ-Al_2O_3 with a remarkably higher amount of DM-BIPs, and the selectivity for the undesulfurized products was closer to that over Co–Mo/V25-Al_2O_3, particularly for the TH- and HH-DMDBTs. As discussed earlier, the rate of the HYD pathway in the DBT HDS was faster than that of the DDS pathway for the Co–Mo/V*x*-Al_2O_3 catalysts but vice versa for the Co–Mo/γ-Al_2O_3 catalyst. For the dual-bed Co–Mo/γ-Al_2O_3||Co–Mo/V25-Al_2O_3 catalyst, the DDS pathway was favorable over the top bed Co–Mo/γ-Al_2O_3 catalyst and contributed most of the desulfurization activity, while the bottom bed Co–Mo/V25-Al_2O_3 catalyst acted as a HYD catalyst for the products coming out of the top catalyst bed. As a result, the product selectivity

was observed as expected for a combination of DDS and HYD pathway. With halved catalyst amount of Co–Mo/γ-Al_2O_3, a worse sulfur removal efficiency was observed.

Over the dual-bed Co–Mo/V25-Al_2O_3||Co–Mo/γ-Al_2O_3 catalyst, the HYD pathway dominated the HDS reaction catalyzed by the top bed of Co–Mo/V25-Al_2O_3 catalyst and the DDS pathway dominated in the bottom bed of Co–Mo/γ-Al_2O_3 catalyst. Undesulfurized TH- and HH-DMDBTs evolving out of the top bed of Co–Mo/V25-Al_2O_3 catalyst were reactive for desulfurization over the bottom bed of Co–Mo/γ-Al_2O_3 via σ adsorption. Therefore, its product selectivity spectrum could be attributed to the superimposed activity of Co–Mo/V25-Al_2O_3 onto Co–Mo/γ-Al_2O_3 and was similar to that over Co–Mo/γ-Al_2O_3 with additional selectivity of the desulfurized product of DM-DICs and for the undesulfurized product of TH- and HH-DMDBTs. The sulfur removal efficiency over Co–Mo/V25-Al_2O_3||Co–Mo/γ-Al_2O_3 was higher than that over Co–Mo/γ-Al_2O_3||Co–Mo/V25-Al_2O_3 with a reversed configuration (Table 6). Those experimental results suggested that the DDS and HYD pathways were catalyzed through σ adsorption and π adsorption via different active sites, respectively. Once the undesulfurized TH-, HH- and DH-DMDBTs that were formed via the HYD pathway were desorbed from π adsorption sites into the gas phase, they were re-adsorbed on σ adsorption sites and desulfurized.

As shown in Table 6, the concerted HYD-DDS pathway of the dual-bed catalyst system could be further verified and improved by suitable arrangement of these two catalysts. Equal amounts of the Co–Mo/γ-Al_2O_3 and Co–Mo/V25-Al_2O_3 particles of 10–20 mesh size were physically mixed into a binary particle system, denoted as Co–Mo/γ-Al_2O_3+Co–Mo/V25-Al_2O_3. At an overall WHSV of 3 h^{-1}, this binary catalyst system showed an improved 46DMDBT conversion up to 85% and a sulfur removal efficiency up to 93%. In the Co–Mo/γ-Al_2O_3+Co–Mo/V25-Al_2O_3 binary catalyst system, the Co–Mo/γ-Al_2O_3 and Co–Mo/V25Al particles contacted each other more closely than in the dual-bed catalyst system. As a result, excessive hydrocracking reactions occurred rendering a high selectivity of cracking products.

A binary powder mixture, denoted as Co–Mo/γ-Al_2O_3///Co–Mo/V25-Al_2O_3, was prepared by grinding the two catalysts into fine powders of equal amounts and re-compressing them into 10–20 mesh particles. The two catalyst components should intimately contact each other. Thus, the distance in the gas phase for intermediates (TH-, HH- and DH-DMDBTs) transported from π adsorption sites to σ adsorption sites is shortened. At an overall WHSV of 3 h^{-1}, the binary powder mixture of Co–Mo/γ-Al_2O_3///Co–Mo/V25-Al_2O_3 showed a higher conversion of 46DMDBT of 87% and a better sulfur removal efficiency of 95% than the binary particle system of Co–Mo/γ-Al_2O_3+Co–Mo/V25-Al_2O_3. The particle mixture and powder mixture catalysts showed distinct different product selectivity of desulfurized products, 77.7% vs. 92.2%, and undesulfurized products, 7.2% vs. 4.9%, indicated their characteristic catalytic behaviors. At an overall WHSV of 1.5 h^{-1} (3 h^{-1} with respect to each catalyst), the powder mixed catalyst gave a higher sulfur removal efficiency of 98% and a much higher 46DMDBT conversion of 100%. Most recently, the research group of Prins developed Pd–Pt/γ-Al_2O_3 and Pt–Pd/mesoporous Na-ZSM-5 catalysts to catalyze the HDS of DBT and 46DMDBT through HYD route reaction pathway [30,33]. Baldovino-Medrano et al. also investigated the HDS of DBT by using Pd–Pt/γ-Al_2O_3 as catalyst [34]. All these studies showed the synergistic effect between the acid function of supports and hydrogenation activity of noble metals for deep desulfurization. Particularly, with chemical synergism between the noble metals and the presence of alloyed particles, bimetallic Pt–Pd catalysts were much more active than the combination of their monometallic constituents [30]. As demonstrated in this study, the concerted HYD-DDS reaction pathway can take place on interparticles. The binary powder mixed catalyst could be useful in producing clean diesel fuel in response to increasingly stringent regulation.

4. Conclusions

Binary oxides V*x*-Al_2O_3 prepared by the co-impregnation method have been demonstrated to be a useful catalyst support for HDS reaction. The pore size distribution of the binary oxide support depends on the vanadia content. A binary oxide support with an appropriate pore diameter of about 100 Å could be obtained by loading 25 wt.% of vanadia content in γ-Al_2O_3.

The XPS spectra confirmed that incorporation of vanadia induced the formation of V–Mo sulfide. Vanadia introduction in catalyst support would decrease the reaction rate of DDS and promote that of HYD for Co–Mo/V*x*-Al_2O_3 catalysts. In contrast to the conventional Co–Mo/γ-Al_2O_3 catalyst, all the Co–Mo/V*x*-Al_2O_3 catalysts preferred the HYD reaction pathway over the DDS pathway in the DBT HDS reaction. The Co–Mo/V25-Al_2O_3 catalyst showed a very high HYD/DDS ratio of 3.4, larger than the value of 0.2 for the traditional Co–Mo/γ-Al_2O_3, higher methylation product selectivity, but lower desulfurization efficiency.

Due to steric hindrance, desulfurization of 46DMDBT through the DDS pathway is not viable. By promoting the HYD reaction pathway, Co–Mo/V25-Al_2O_3 was found effective in catalyzing 46DMDBT conversion in which 46DMDBT was converted into naphthenic compounds with lower steric hindrance. A synergistic effect of the DDS pathway and the HYD pathway was achieved by using binary catalyst systems comprising Co–Mo oxide catalysts supported both on γ-Al_2O_3 and V25-Al_2O_3 to allow hydrogenated species to be desulfurized on the Co–Mo sulfide catalysts. An optimum catalyst system was prepared through powder mixing to allow intimate contact between the different catalyst components. By means of concerted HYD-DDS pathway, the binary powder system could effectively convert the most refractory sulfur compound 46DMDBT at a high HDS conversion and high sulfur removal efficiency into a clean diesel fuel.

Acknowledgments

We gratefully thank the National Science Council, Taiwan, ROC for financial supports of this work (NSC 97-2221-E-007-051). We also thank Dr. H.W. Jen for stimulated discussions.

References

[1] M. Houalla, N.K. Nag, A.V. Sapre, D.H. Broderick, B.C. Gates, AIChE J. 24 (1978) 1015.
[2] G.H. Singhal, R.L. Espino, J.E. Sobel, G.A. Huff, J. Catal. 67 (1981) 457.
[3] T. Kabe, A. Ishihara, Q. Zhang, Appl. Catal. A: Gen. 97 (1993) L1.
[4] X.L. Ma, K. Sakanishi, I. Mochida, Ind. Eng. Chem. Res. 33 (1994) 218.
[5] K. Segawa, K. Takahashi, S. Satoh, Catal. Today 63 (2000) 123.
[6] M. Daage, R.R. Chianelli, J. Catal. 149 (1994) 414.
[7] M. Egorova, R. Prins, J. Catal. 225 (2004) 417.
[8] B.C. Gates, H. Topsøe, Polyhedron 16 (1997) 3213.
[9] A. Nishijima, H. Shimada, T. Sato, Y. Yoshimura, N. Matsubayashi, T. Kameoka, J. Jpn. Petrol. Inst. (Sekiyu Gakkaishi) 32 (1989) 35.
[10] T.A. Pecoraro, R.R. Chianelli, J. Catal. 67 (1981) 430.
[11] M. Lacroix, N. Boutarfa, C. Guillard, M. Vrinat, M. Breysse, J. Catal. 120 (1989) 473.
[12] S. DeJonghe, R. Hubaut, J. Grimblot, J.P. Bonnelle, T. DesCourueres, D. Faure, Catal. Today 7 (1990) 569.
[13] M. Lacroix, C. Guillard, M. Breysse, M. Vrinat, T. Des Courierès, J. Catal. 135 (1992) 304.
[14] A. Thiollier, P. Afanasiev, M. Cattenot, M. Vrinat, Catal. Lett. 55 (1998) 39.
[15] I. Wang, R.C. Chang, J. Catal. 117 (1989) 266.
[16] C.M. Wang, T.C. Tsai, I. Wang, J. Catal. 262 (2009) 206.
[17] N. Blangenois, M. Florea, P. Grange, R.P. Silvy, S.P. Chenakin, jean M. Bastin, N. Kruse, B.P. Barbero, L. Cadús, Appl. Catal. A: Gen. 263 (2004) 163.
[18] C.J. Brinker, G.W. Scherer, Sol–Gel Science, The Physics and Chemistry of Sol–Gel Processing, Acad. Press Inc., Harcourt Brace Jovanocich Publisher, 1990, pp. 31–35, 59–77.
[19] K.V.R. Chary, G. Kishan, J. Phys. Chem. 99 (1995) 14424.

[20] B.M. Reddy, B. Chowdhury, E.P. Reddy, A. Fernández, J. Mol. Catal. A: Chem. 162 (2000) 431.
[21] B.M. Reddy, B. Chowdhury, E.P. Reddy, A. Fernández, Appl. Catal. A: Gen. 213 (2001) 279.
[22] G.S. Wong, M.R. Concepcion, J.M. Vohs, Surf. Sci. 526 (2003) 211.
[23] J. Mendialdua, R. Casanova, Y. Barbaux, J. Electron Spectrosc. Relat. Phenom. 71 (1995) 249.
[24] F. Bataille, J.L. Lemberton, G. Perot, P. Leyrit, T. Cseri, N. Marchal, S. Kasztelan, Appl. Catal. A: Gen. 220 (2001) 191.
[25] D.D. Whitehurst, T. Isoda, I. Mochida, Adv. Catal. 42 (1998) 345.
[26] T.C. Ho, J. Catal. 219 (2003) 442.
[27] M. Egorova, R. Prins, J. Catal. 224 (2004) 278.
[28] C.I. Chu, I. Wang, Ind. Eng. Chem. Process Des. Dev. 21 (1982) 338.
[29] A. Röthlisberger, R. Prins, J. Catal. 235 (2005) 229.
[30] A. Röthlisberger, R. Prins, J. Catal. 242 (2006) 207.
[31] X.L. Ma, K. Sakanishi, I. Mochida, Ind. Eng. Chem. Res. 35 (1996) 2487.
[32] M. Egorova, R. Prins, J. Catal. 221 (2004) 11.
[33] Y.Y. Sun, R. Prins, Angew. Chem. Int. Ed. 47 (2008) 8478.
[34] V.G. Baldovino-Medrano, P. Eloy, E.M. Gaigneaux, S.A. Giraldo, A. Centeno, J. Catal. 267 (2009) 129.